NANO LETTERS

Letter

pubs.acs.org/NanoLett

Uniform Nano-Sn/C Composite Anodes for Lithium Ion Batteries

Yunhua Xu,[†,§] Qing Liu,[‡,§] Yujie Zhu,[†] Yihang Liu,[†] Alex Langrock,[†] Michael R. Zachariah,*[,‡] and Chunsheng Wang*[,†]

[†]Department of Chemical and Biomolecular Engineering and [‡]Department of Chemistry and Biochemistry, University of Maryland, College Park, Maryland 20742, United States

Supporting Information

ABSTRACT: Nano-Sn/C composites are ideal anode materials for high energy and power density Li-ion batteries. However, because of the low melting point of Sn and the tendency of grain growth, especially during high temperature carbonization, it has been a significant challenge to create well-dispersed ultrasmall Sn nanoparticles within a carbon matrix. In this paper, we demonstrate an aerosol spray pyrolysis technique, as a facile and scalable method, to synthesize a nano-Sn/C composite with uniformly dispersed 10 nm nano-Sn within a spherical carbon matrix. The discharge capacity of nano-Sn/C composite sphere anodes maintains the initial capacity of 710 mAh/g after 130 cycles at 0.25 C. The nano-Sn/C composite sphere anodes can provide ~600 mAh/g even at a high rate of 20 C. To the best of our knowledge, such high rate performance for Sn anodes has not been reported previously. The exceptional performance of the nano-Sn/C composite is attributed to the unique nano-Sn/C structure: (1) carbon matrix offers mechanical support to accommodate the stress associated with the large volume change of nano-Sn, thus alleviating pulverization; (2) the carbon matrix prevents Sn nanoparticle agglomeration upon prolonged cycling; and (3) carbon network provides continuous path for Li ions and electrons inside the nano-Sn/C composite spheres.

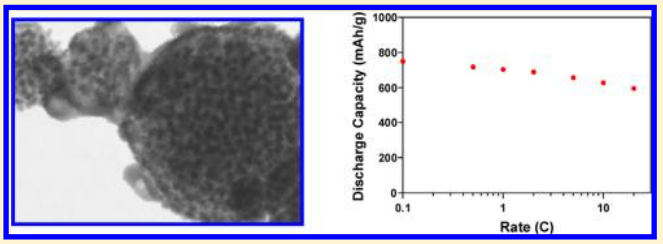

KEYWORDS: *Tin nanoparticle, aerosol spray pyrolysis, anode, energy storage, lithium-ion battery*

Rechargeable lithium-ion batteries have been widely used in mobile electronic devices. To apply Li-ion batteries in electric vehicles and renewable energy storage, a significant advance in energy storage density, power density, and cycle life is required.[1] Current Li-ion batteries use graphite anodes in which one unit (six carbon atoms for graphite) can store one or less lithium ion, leading to a limited theoretical capacity of 372 mAh/g.[2,3] To circumvent the low energy and power density of graphite, alternative materials are highly desired.

Tin anodes have attracted much attention because it delivers a capacity up to three times higher than that of graphite.[4−19] Theoretically, one tin atom can maximally react with 4.4 lithium atoms to form $Li_{4.4}Sn$ alloy, reaching a capacity of 993 mAh/g.[8] However, the large amount of lithium insertion/extraction into/from Sn causes a large volume change (about 300%), which causes pulverization of tin particles and loss of contact with current collector, resulting in poor electrochemical performance.[20,21]

Extensive efforts have been made to improve the electrochemical behavior of Sn anodes. The most effective approaches include (1) reducing Sn particle size to nanoscale (<10 nm) to efficiently mitigate the absolute strain induced by the large volume change during lithiation/delithiation, and retard particle pulverization;[12,14,22,23] (2) using nano-Sn with uniform particle size (narrow size distribution) to generate uniform stress/strain over the entire electrode during lithiation/delithiation, preventing local cracking;[22] (3) uniformly dispersing nano-Sn in a conductive matrix (such as carbon) to accommodate volume change and maintain the mechanical integrity of the composite electrode.[12,14,15] Clearly, a Sn/C composite with uniform tin nanoparticles (<10 nm) dispersed in a carbon matrix would be an ideal anode for Li-ion batteries. For example, Scrosati and co-workers synthesized a nanostructured Sn/C composite by infiltrating tin precursor into an organic gel, followed by carbonization at a high temperature.[12,14] The nanostructured Sn/C composite can be charged/discharged for more than 100 cycles.[12,14] Very recently, we reported a spongelike porous C/Sn composite synthesized by dispersing SnO_2 nanoparticles into a soft-template polymer matrix followed by carbonization, and good electrochemical performance was demonstrated.[24] However, it is a significant challenge to control the nano-Sn particle size and uniformity of Sn particle dispersion in the carbon matrix using current synthesis technology because of the low melting point of Sn, which aggravate liquid coalescence during extended carbonization.

In this paper, we introduce aerosol spray pyrolysis to realize the ideal structure with nanograin Sn uniformly dispersed in a spherical conductive carbon matrix (Figure 1a). The successful key of this method is rooted in the rapid heating of precursor droplets, which allows quick formation of Sn nanograins and carbon frame. The short residence time and rapid subsequent

Received: October 15, 2012
Revised: December 8, 2012
Published: January 2, 2013

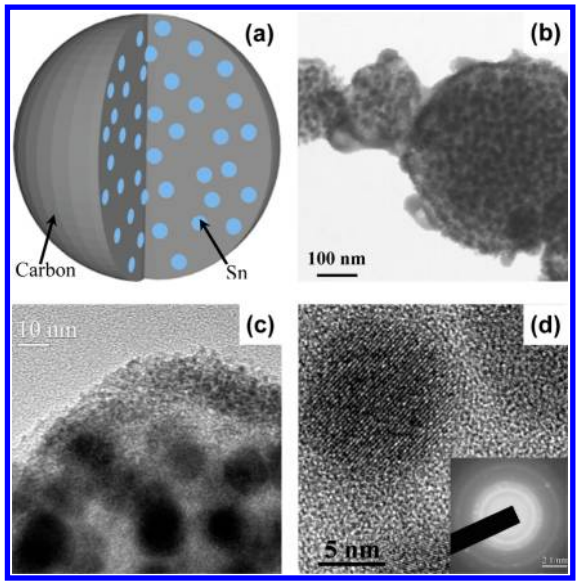

Figure 1. (a) Schematic diagram, (b) TEM image, and (c,d) high-resolution images of the nano-Sn/C composite particles. Insert: SAED image.

cooling enables one to freeze the structure to nonaggregated and uniformly sized nano-Sn grains in a carbon matrix. Even though the melting point of Sn is lower than the carbonization temperature, Sn nucleation occurs rapidly and grain growth terminates at about 10 nm (Figure 1b–d). In addition, the fast formation of the carbon network is another factor that prevents Sn grains from growing bigger. By contrast, traditional synthesis cannot shorten the heating time to second level, which inevitably sinters the Sn grains. Therefore, aerosol spray pyrolysis method is a powerful technique to synthesize Sn/C composite with uniformly dispersed Sn nanoparticles in the carbon matrix. The nano-Sn/C composite spheres demonstrated exceptional rate performance and cycling stability.

Nano-Sn/C composite spheres were synthesized by aerosol spray pyrolysis. $SnCl_2$ and polyvinylpyrrolidone (PVP) were used as Sn and C sources, respectively, and dissolved into ethanol to form a precursor solution, which was atomized with argon/5% hydrogen flow by a collision-type nebulizer. The aerosol was dried and subsequently decomposed in a tubular furnace at 900 °C. Thermal decomposition of Sn source along with carbonization of polymer yields nano-Sn/C composite spheres.

Figure 1b–d shows transmission electron microscopy (TEM) images of the nano-Sn/C composite spheres synthesized by aerosol spray pyrolysis. It is clearly seen that uniform-sized tin nanoparticles are well dispersed in the spherical carbon matrix. The lighter color in the spheres represents the carbon frame, and the darker color represents the metallic Sn particles. The high-resolution TEM images (Figure 1c,d) reveal that the Sn nanoparticles in the composite spheres are around 10 nm, and a thin layer (~10 nm) of carbon is coated on the surface of the nano-Sn/C composite spheres (Figure 1c).

The crystal structure of the nano-Sn/C composite was investigated using X-ray diffraction (XRD) (Supporting Information Figure S1) and selected area electron diffraction (SAED) (insert in Figure 1d). All the peaks in the XRD pattern can be well indexed to a tin crystal structure (JCPDS card No.: 862265). No SnO_2 is detected in the nano-Sn/C composite because (1) using ethanol as the precursor solvent, no hydrolysis occurs, which is the primary reaction of the forming SnO_2, and (2) spray pyrolysis is conducted in reducing atmosphere of Ar/H_2. The crystal structure was confirmed by the SAED image, shown in the insert of Figure 1d. The bright diffraction rings in the SAED image indicates the typical feature of crystal structure.

The composition analysis of the spherical nano-Sn/C composite was performed with TGA in air. (Data are shown in Supporting Information Figure S2.) Almost no weight loss was observed from 100 to 220 °C, demonstrating that the composite is stable up to 220 °C in air, that is, there is no Sn oxidation reaction and carbon decomposition at a temperature of lower than 220 °C. The weight increase from 220 to 300 °C is attributed to the oxidation of metallic tin ($Sn + O_2 \rightarrow SnO_2$), while the followed weight loss from 300 to 540 °C is mainly due to the carbon decomposition to carbon dioxide ($C + O_2 \rightarrow CO_2$ (gas)). Assuming that the TGA heating finally produces SnO_2, the content of nano-Sn particles in the composite is determined to be 62% based on the following equation:

$$\mathrm{Sn(wt\%)} = 100 \times \frac{\text{molecular weight of Sn}}{\text{molecular weight of } SnO_2} \times \frac{\text{final weight of } SnO_2}{\text{initial weight of nano-Sn/C composite}}$$

Aerosol spray pyrolysis is one-step and droplet-to-particle method. The formation mechanism of nano-Sn/C composite in aerosol spray pyrolysis process is proposed and summarized in Figure 2. In a typical process, precursor solution was atomized into microsized droplets and then was swept by a carrier gas consequently through a dryer to form precursor particles and a high-temperature furnace to pyrolysis. In the furnace, precursor particles suffered a quick heating up and cooling down process to finally produce the composite. The size of precursor particles was mainly determined by the atomizer and concentration of the precursor solution. The particle size distribution of the nano-Sn/C composite was measured using online differential mobility analysis, and the data are included in Supporting Information Figure S3. The results reveal that the composite has a peak at 114 nm in particle size distribution, which is a common feature for aerosol-synthesized particles.

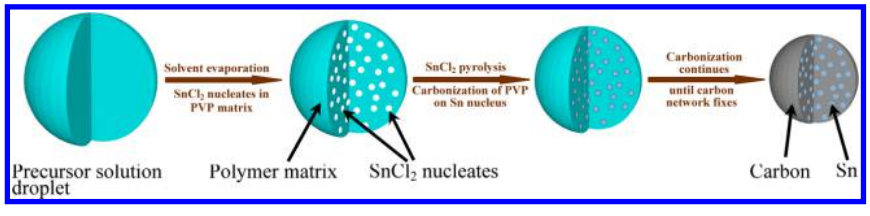

Figure 2. Schematic formation processes of ultrasmall nano-Sn dispersed carbon spheres.

dx.doi.org/10.1021/nl303823k | *Nano Lett.* 2013, 13, 470–474

It has been reported that metal or metal salt is required in the precursor solution to produce carbon materials by spray pyrolysis.[25] In this case, Sn grains function as catalysts to promote the formation of carbon, while the carbon frame and the short residence time in the furnace suppress the growth of Sn grains, thus forming a uniform nano Sn/C composite. As the aerosol that contains solid particles after solvent evaporation flew into the furnace at a high temperature of 900 °C, $SnCl_2$ was decomposed to Sn under the Ar/H_2 environment. The Sn nuclei grow through diffusion-coalescence processes since Sn is in molten state at this point. The growth is determined by the precursor composition and heating residence time. Simultaneously, one expects the polymer pyrolysis and dehydrogenation to lead to carbon formation. The short residence time (~1 s) in the high-temperature furnace limits the growth of the Sn nuclei. Under these conditions a large number of Sn nuclei are formed, which presumably provides more active sites for carbonization and carbon deposition. The solvent evaporation forms the droplet periphery leading to a local increase in solute concentration and local precipitation, which results in a less dense material.

Porosity of spray-pyrolysis synthesized particles cannot be easily observed under TEM, or measured by traditional BET methods because the closed pores will not allow N_2 to access. Alternatively, the porosity can be estimated by measuring the particle density and comparing it with the theoretical value derived from the component ratio by TGA. In a prior work it has been demonstrated that the tandem differential mobility-particle mass analysis (DMA-APM) method is a robust measure of porosity since it determines porosity from density rather than gas permeation (i.e., BET).[26] The density measurement of the product aerosol particles were conducted at different sizes of 30, 50, 100, and 200 nm by online tandem DMA-APM. It is found that the particle density increases with decrease in particle size, 4050 kg/m^3 for 100 nm, 6400 kg/m^3 for 50 nm, and 7050 kg/m^3 for 30 nm, respectively. While as the particle size is larger than 150 nm, a constant density of about 2900 kg/m^3 was observed. The particle size distribution has a peak at 114 nm (in Supporting Information Figure S2), which is larger than 100 nm. So the average density of the nano-Sn/C composite particles should be smaller than 4050 kg/m^3. However, providing density of Sn is 7400 kg/m^3 and that of carbon is about 2300 kg/m^3, the calculated density of the nano-Sn/C composite is about 5500 kg/m^3 according to TGA percentage data (62% of Sn and 38% of carbon by mass), which is much larger than the average density measured by tandem DMA-APM method. The lower particle density measured by the tandem DMA-APM method strongly suggests that the particles have a porous structure, which provides additional space to accommodate the volume change.

Electrochemical performance of the nano-Sn/C composite electrodes was investigated in coin cells using lithium as the counter electrode. Figure 3a shows cyclic voltammograms of the initial 5 cycles at a scan rate of 0.1 mV/s between 0 and 3 V. Three small reduction peaks at 0.2, 0.37, and 0.57 V are assigned to the lithium insertion into tin to form a Li_xSn alloy. Oxidation peaks at 0.53, 0.67, and 0.8 V correspond to the delithiation reaction of Li_xSn alloy. The broad anodic peak at 1.2 V represents lithium extraction from carbon.[11,24] The difference between the first and the second cathodic scans is mainly attributed to the decomposition of the electrolyte to form solid-electrolyte interface (SEI) films. The unchanged peak current intensity, except the first cycle, implies good

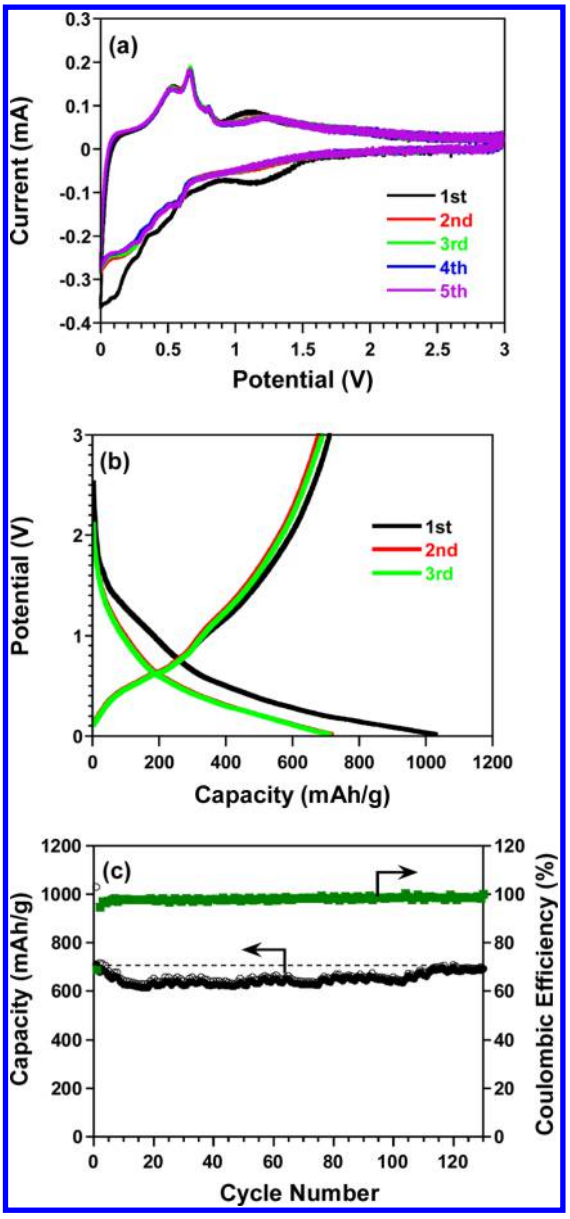

Figure 3. (a) Cyclic voltammograms of the initial 5 cycles scanned between 0–3 V at a rate of 0.1 mV/s, (b) charge/discharge profiles at the initial three cycles, and (c) cycling performance at 0.02–3 V and 200 mA/g of the nano-Sn/C composite.

cycling stability of the nano-Sn/C composite. The voltage profiles of nano-Sn/C anodes in the initial three charge/discharge cycles between 0.02 and 3.0 V at the current density of 200 mA/g (0.26 C) are shown in Figure 3b. The first lithiation delivers a capacity of 1029 mAh/g and 69% of the inserted Li can be reversibly delithiated, providing charge capacity of 710 mAh/g. The first delithiation capacity is close to the theoretical capacity (756 mAh/g) of the nano-Sn/C composite if we assume carbon delivers the capacity of 372 mAh/g. The capacity loss of 319 mAh/g in the first cycle is mainly attributed to the formation of SEI film. The repeatable charge/discharge curves after the first cycle demonstrate good cycling stability.

The highly uniform nano-Sn/C composite spheres not only fully utilize the Sn nanoparticles to store lithium ions, thus providing high capacity, but also improves the cycling stability. Figure 3c shows the cycling performance of the nano-Sn/C

dx.doi.org/10.1021/nl303823k | Nano Lett. 2013, 13, 470–474

composite during charge/discharge processes between 0.02 and 3.0 V at the current density of 200 mA/g. The nano-Sn/C composite exhibits exceptional cycling stability during 130 charge/discharge cycles with slight capacity decay in the first 10 cycles. The Coulombic efficiency approaches 100% after 10 cycles, showing excellent reversibility of the nano-Sn/C composite. The superior cycling performance is attributed to three unique features of the nano-Sn/C composite spheres. First is the ultrasmall size of tin nanoparticles. It has been shown that reduced particle size can significantly reduce the strain and improve the electrochemical property of electrode materials. Second, the carbon frame, which acts to release strain, can accommodate the large volume change and prevent metal aggregation over repeated cycling. Finally, the uniform distribution of tin nanoparticles in the carbon frame is an important factor to generate a balanced stress over the whole composite particles and electrode and thus enhances long-term electrochemical performance. The robustness of the nano-Sn/C anode structure is also evidenced by the ~100% Coulombic efficiency after 10 cycles.

Since ultrasmall Sn nanoparticles (10 nm) are uniformly distributed in the spherical carbon matrix, high rate capacity is anticipated. The rate capability of the nano-Sn/C composite anodes were measured using three protocols:

(1) Discharge rate capability. Charge (lithiation) at the same rate of 0.1 C while discharge (delithiation) at different C rates.

(2) Charge rate capability. Discharge at the same rate of 0.1 C while charge at different C rates.

(3) Charge/discharge rate capability. Both charge and discharge at different C rates.

Figure 4 presents the rate capacities under the three charge/discharge protocols. The nano-Sn/C composite demonstrated

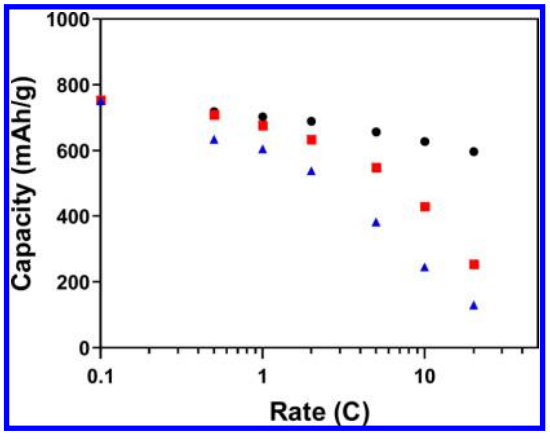

Figure 4. Rate performance of the nano-Sn/C composite at different test conditions. (a) Charge at 0.1 C and discharge at different rates from 0.1 to 20 C; (b) charge at different rates from 0.1 to 20 C and discharge at 0.1 C; (c) charge and discharge at the same rates from 0.1 to 20 C.

excellent discharge rate capability. At 20 C (C rate = 756 mA/g), the discharge capacity retention is still as high as about 600 mAh/g, corresponding to 80% of that at 0.1 C. This also indicates that 97% of inserted lithium ions at 0.1 C can be extracted even at a high delithiation rate of 20 C. Such a high rate behavior has never been reported in literatures for Sn anodes. The exceptional high discharge capability of nano-Sn/C composites demonstrated a significant advance in Li-ion battery technologies because the discharge power density is critical for most practical applications. The charge rate capacity was also examined by discharging at the same rate of 0.1 C but charging at different rates from 0.1 to 20 C (Figure 4). It can be seen that at low rates (less than 1 C), there is no obvious capacity difference between the charge and discharge rate capabilities. When the C rate was increased to higher than 1 C, the charge rate capacity declined faster than the discharge rate capacity. The charge capacity is only 300 mAh/g at 20 C, which is half of the discharge capacity at the same C rate. The difference between discharge and charge capabilities is attributed to the larger reaction voltage window in discharge (ΔV_{dis}, voltage difference between average delithiation voltage at 0.1 C and cutoff voltage) than that (ΔV_{ch}, voltage difference between average lithiation voltage at 0.1 C and cutoff voltage) in charge (Supporting Information Figure S5b). The amount of Li ions that can be extracted/inserted from/in nano-Sn/C composite spheres at a high C rate depends on the ratio of overpotential to reaction voltage window ($\eta/\Delta V$). Assuming that the overpotentials (η) for charge and discharge are the same, the larger voltage window in discharge than in charge ($\Delta V_{dis} > \Delta V_{ch}$) allows more lithium ions to be extracted but less to be inserted at the same C rate. The charge/discharge rate capability of Sn/C composite is slightly worse than charge rate capability. Actually, in practical applications, the discharge rate capability is more important than the charge rate performance. The exceptional discharge rate capability of the nano-Sn/C composite makes it promising and attractive for applications requiring high power and high energy density.

The morphology changes of nano-Sn/C composite after 50 charge/discharge cycles between 0.02 and 3.0 V at 200 mA/g current were investigated using TEM (Figure 5). In comparison

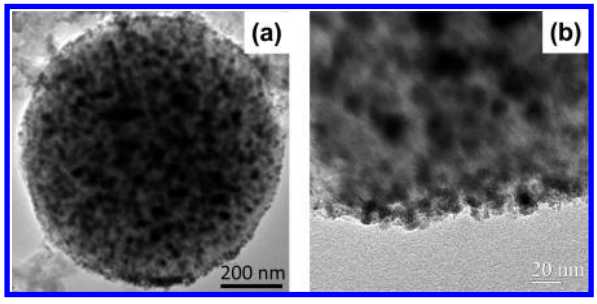

Figure 5. TEM images of the nano-Sn/C composite after 50 charge/discharge cycles.

to the morphology of the fresh nano-Sn/C composite anode in Figure 1, no obvious morphology change was observed after 50 charge/discharge cycles. The spherical shape of the nano-Sn/C spheres was sustained as a whole integration structure, suggesting that the carbon matrix can effectively accommodate the volume change and alleviate the strain during the insertion/deinsertion reactions. We also observed that the tin nanoparticles still retain nano-Sn/C composite morphology with a uniform distribution (Figure 5a), indicating that the pulverization and aggregation commonly observed for tin-based anode materials were substantially reduced.

In conclusion, nano-Sn/C composites were synthesized using aerosol spray pyrolysis as anode material for lithium-ion batteries. Because of the fast carbonization of the carbon precursor under the catalytic effects of metallic Sn and very short carbonization time at high temperature during the aerosol spray pyrolysis process, ultrasmall Sn grains with uniform size

dx.doi.org/10.1021/nl303823k | Nano Lett. 2013, 13, 470−474

were homogenously dispersed in a spherical carbon matrix. The unique structure can effectively alleviate stress and accommodate large volume changes, as well as prevent the pulverization and agglomeration of Sn grains upon prolonged cycling. The nano-Sn/C composite showed a reversible capacity of 710 mAh/g, and there is no capacity fading even after 130 charge/discharge cycles at 200 mAh/g. More importantly, exceptional rate capability was demonstrated for the nano-Sn/C composite without significant capacity loss at a discharge rate as high as 20 C. The electrochemical performance is superior to the nano-Sn/C composite anodes synthesized using other techniques. Meanwhile, the synthesis of aerosol spray pyrolysis is a widely used technique for commercial nanomaterials and easily scaled up, making nano-Sn/C composite very promising and attractive as an anode material for lithium-ion batteries.

■ ASSOCIATED CONTENT

Supporting Information

Additional information and figures. This material is available free of charge via the Internet at http://pubs.acs.org.

■ AUTHOR INFORMATION

Corresponding Author

*E-mail: (C.W.) cswang@umd.edu; (M.R.Z.) mrz@umd.edu.

Author Contributions

§These authors contributed to this work equally.

Notes

The authors declare no competing financial interest.

■ ACKNOWLEDGMENTS

The authors gratefully acknowledge the support of the Army Research Office under Contract No.: W911NF1110231 (Dr. Robert Mantz, Program Manager) and Ellen Williams Distinguished Postdoctoral Fellowship.

■ REFERENCES

(1) Kasavajjula, U.; Wang, C. S.; Appleby, A. J. *J. Power Sources* **2007**, *163*, 1003.
(2) Dahn, J. R.; Zheng, T.; Liu, Y.; Xue, J. S. *Science* **1995**, *270*, 590.
(3) Dresselhaus, M. S.; Dresselhaus, G. *Adv. Phys.* **1981**, *30*, 139.
(4) Kim, M. G.; Cho, J. *Adv. Funct. Mater.* **2010**, *19*, 1497.
(5) Zou, Y. Q.; Wang, Y. *ACS Nano* **2011**, *5*, 8108.
(6) Luo, B.; Wang, B.; Liang, M.; Ning, J.; Li, X.; Zhi, L. *Adv. Mater.* **2012**, *24*, 1405.
(7) Hassoun, J.; Lee, K.-S.; Sun, Y.-K.; Scrosati, B. *J. Am. Chem. Soc.* **2011**, *133*, 3139.
(8) Winter, M.; Besenhard, J. O. *Electrochim. Acta* **1999**, *45*, 31.
(9) Lee, K. T.; Jung, Y. S.; Oh, S. M. *J. Am. Chem. Soc.* **2003**, *125*, 5652.
(10) Kim, I.; Blomgren, G. E.; Kumta, P. N. *Electrochem. Solid-State Lett.* **2004**, *7*, A44.
(11) Jung, Y. S.; Lee, K. T.; Ryu, J. H.; Im, D.; Oh, S. M. *J. Electrochem. Soc.* **2005**, *152*, A1452.
(12) Derrien, G.; Hassoun, J.; Panero, S.; Scrosati, B. *Adv. Mater.* **2007**, *19*, 2336.
(13) Zhang, W. M.; Hu, J. S.; Guo, Y. G.; Zheng, S. F.; Zhong, L. S.; Song, W. G.; Wan, L. J. *Adv. Mater.* **2008**, *20*, 1160.
(14) Hassoun, J.; Derrien, G.; Panero, S.; Scrosati, B. A. *Adv. Mater.* **2008**, *20*, 3169.
(15) Yu, Y.; Gu, L.; Zhu, C. B.; Aken, P. A.; Maier, J. *J. Am. Chem. Soc.* **2009**, *131*, 15984.
(16) Yu, Y.; Gu, L.; Wang, C. L.; Dhanabalan, A.; Aken, P. A.; Maier, J. *Angew. Chem., Int. Ed.* **2009**, *48*, 6485.
(17) Kim, M. G.; Sim, S.; Cho, J. *Adv. Mater.* **2010**, *22*, 5154.
(18) Li, M.-Y.; Liu, C.-L.; Wang, Y.; Dong, W.-S. *J. Electrochem. Soc.* **2011**, *158*, A296.
(19) Li, X.; Dhanabalan, A.; Wang, C. *Adv. Energy Mater.* **2012**, *2*, 238.
(20) Mao, O.; Dunlap, R. A.; Dahn, J. R. *J. Electrochem. Soc.* **1999**, *146*, 405.
(21) Li, H.; Shi, L.; Lu, W.; Huang, X.; Chen, L. *J. Electrochem. Soc.* **2001**, *148*, A915.
(22) Wang, Y.; Lee, J. Y.; Deivaraj, T. C. *J. Electrochem. Soc.* **2004**, *151*, A1804.
(23) Li, H.; Shi, L.; Wang, Q.; Chen, L.; Huang, X. *Solid State Ionics* **2002**, *148*, 247.
(24) Xu, Y. H.; Guo, J. C.; Wang, C. S. J. *J. Mater. Chem.* **2012**, *22*, 9562.
(25) Sunkara, B.; Zhan, J.; Kolesnichenko, I.; Wang, Y.; He, J.; Holland, J. E.; McPherson, G. L.; John, V. T. *Langmuir* **2011**, *27*, 7854.
(26) Liu, Q.; Ma, X.; Zachariah, M. R. *Microporous Mesoporous Mater.* **2012**, *153*, 210.